Journal of Asian Ceramic Societies

High-temperature toughening in ternary high-entropy (Ta1/3Ti1/3Zr1/3)C carbide consolidated using spark-plasma sintering

--Manuscript Draft--

Full Title:	High-temperature toughening in ternary high-entropy (Ta1/3Ti1/3Zr1/3)C carbide consolidated using spark-plasma sintering
Manuscript Number:	
Article Type:	Full Length Article
Keywords:	tantalum carbide; high-entropy ceramics; flexural strength; toughness; high-temperature materials
Abstract:	We report for the first time the effect of temperature on the mechanical properties of (Ta 1/3 Ti 1/3 Zr 1/3)C carbide. Flexural strength and fracture toughness were investigated using the three-point bending technique in argon. Using commercially-available carbide powders with an equimolar ratio and performing spark plasma consolidation at 1973 °C, we obtained a bulk single-phase high-entropy carbide ceramic with the lattice parameter a = 4.458 Å. The flexural strength and fracture toughness at room temperature reached on average 700 MPa and 3.2 MPa m 1/2 , respectively. At 1800 °C, local decomposition of the high-entropy carbide took place as a structure with a local chemical gradient was observed after high-temperature tests, which increased fracture toughness by 30% (to 4.4 MPa m 1/2).
Order of Authors:	Dmytro Demirskyi, Ph.D.
	Toshiyuki Nishimura
	Tohru Suzuki
	Yoshio Sakka
	Oleg Vasylkiv
	Kyosuke Yoshimi

High-temperature toughening in ternary high-entropy $(Ta_{1/3}Ti_{1/3}Zr_{1/3})C$ carbide consolidated using spark-plasma sintering

D. Demirskyi (a,b,c)†, T. Nishimura (b), T.S. Suzuki (b), Y. Sakka (b), O. Vasylkiv (b)†, and K. Yoshimi (c).

(a) WPI-Advanced Institute for Materials Research (WPI-AIMR), Tohoku University, 2-1-1 Katahira, Aoba-ku, Sendai, 980-8577 Japan
(b) National Institute for Materials Science, 1-2-1 Sengen, Tsukuba, Ibaraki 305-0047, Japan
(c) Department of Materials Science and Engineering, Tohoku University, 6-6-02 Aramaki Aza Aoba, Sendai, 980-8579, Japan

Abstract

We report for the first time the effect of temperature on the mechanical properties of $(Ta_{1/3}Ti_{1/3}Zr_{1/3})C$ carbide. Flexural strength and fracture toughness were investigated using the three-point bending technique in argon. Using commercially-available carbide powders with an equimolar ratio and performing spark plasma consolidation at 1973 °C, we obtained a bulk single-phase high-entropy carbide ceramic with the lattice parameter a = 4.458 Å. The flexural strength and fracture toughness at room temperature reached on average 700 MPa and 3.2 MPa $m^{1/2}$, respectively. At 1800 °C, local decomposition of the high-entropy carbide took place as a structure with a local chemical gradient was observed after high-temperature tests, which increased fracture toughness by 30% (to 4.4 MPa $m^{1/2}$).

† Authors to whom correspondence should be addressed, Dmytro Demirskyi, demirskyi.dmytro.e2@tohoku.ac.jp, Oleg Vasylkiv oleg.vasylkiv@nims.go.jp

Keywords: tantalum carbide; high-entropy ceramics; flexural strength; toughness; high-temperature materials.

1 Introduction

Recent progress in high-temperature ceramics based on the solid-solution of transition metal carbides, diborides, and silicides has spurred world wide research for a new class of ultra-high temperature ceramics (UHTC) [1–4]. Analogous to the recent advances in metallurgy [5], they were defined as high-entropy ceramics [8–10]. Various methods of development of multi-metal solid-solution high-entropy ceramics have been reported in the last two years [7–10], but due to the slow atomic mobility of transition metals of the IV and V groups, their consolidation or combined consolidation/synthesis [9] requires the temperature range typical for classical UHTCs (>1800 °C).

Despite reports of the high-hardness and high Young's modulus of high-entropy carbides [11–14], studies related to the strength or toughness at room or high temperature are somehow limited [8,10]. A report of the ternary high-entropy (Ta,Zr,Nb)C [8] showed an interesting high-temperature flexural behavior, suggesting that solid-solution strengthening might lead to further improvement of the high-temperature properties. In this regard, further studies of the ternary or quaternary solid-solution of carbides may clarify the potential development of high-entropy carbides in particular, and the UHTC in general.

Furthermore, for some temperature ranges, binary [15,16] and ternary [17] solid-solutions based on TiC and ZrC will be a distinctive two-phase ceramic. This is a feature that is known if one uses WC or VC in ternary carbide alloys [18]. In addition, for high-entropy ceramics, the layer-by-layer oxidation behavior of the high-entropy ceramics have been reported [19], suggesting that upon reheating to elevated temperatures, the different diffusion rates for metal and carbon atoms in the pure metals or carbides [4] may lead to localization or decomposition of the solid-solution high-entropy ceramics.

The impact of *these phenomena* on the mechanical properties is still unclear. Thus present investigation will examine the possibility of using ternary solid-solution ceramics based on TiC and ZrC as structural materials at elevated temperatures. In particular, the high-temperature flexural strength and fracture toughness of (Ta,Ti,Zr)C was the main focus of this study.

2 Materials and Methods

Commercially-available TaC, TiC, and ZrC (Wako Pure Chemicals, Osaka, Japan) powders were used as the starting materials. The raw powders were mixed in ethanol in equimolar ratios of TaC:TiC:ZrC 1:1:1. For simplicity, a ternary equimolar carbide mixture was denoted as TTZ. Based on the previous results for (Ta,Zr,Nb)C [8], a dwell time of 10 min at 1973 °C was used.

The spark plasma sintering (SPS) experiments were conducted using the 'Dr. Sinter' 1050 (Sumitomo, Japan) unit with a 30-mm die. The schedule for the TTZ

carbide specimens prepared in this study had four major steps: (1) heating to 700 °C in four minutes following a five-minute dwell, (2) heating to 1500 °C in 10 minutes with a five-minute dwell; (3) five-minute ramp to 1973 °C, with the dwell of 10 minutes. The last step included cooling down to 600 °C in 15 minutes. Steps (1) and (2) were performed in a vacuum; during the dwell at 1400 °C, the SPS chamber was backfilled with argon. At the end of the dwell at stage (2), the pressure was increased from 8 to 12 kN, while reaching 1927 °C, the pressure was increased from 12 to 32 kN. The pressure of 32 kN was maintained during the consolidation and cooling stages. Argon gas at the flow rate of 2 L/min was used.

An X-ray diffraction (XRD) analysis (D8 Advance, Bruker, Karlsruhe, Germany) was performed on the polished surfaces of the bars after the flexural tests using Cu-Kα radiation. The intensity data were collected over the 2θ range of 20°–130°, in steps of 0.02–0.05° using a sampling time of 10 s for each step. The software used for refinement was TOPAS (TOPAS Ver. 4.0, Bruker AXS, Germany). Instrumental broadening was determined using a NIST 660b LaB_6 standard run under the same conditions for each carbide sample [20]. The lattice parameters of the carbides were determined with an accuracy of 0.0001 Å.

The structural characteristics of the TTZ ceramics and were studied using scanning electron microscopy (SEM, JCM-6000, JEOL) with secondary (SE) and backscattered electrons (BSE mode).

The three-point flexural strength was determined using rectangular blocks (2×2×25 and 2×2.5×25 mm) and strength testing equipment were previously described in detail [21,22]. A span of 16 mm was used. The fracture toughness of the ceramics was evaluated using specimen bending testing which contained a single edge through-thickness notch following ASTM C1421–10. Details of the testing configuration and the notch profile are presented in ref. [23]. Tests were performed using loading rates of 0.05 or 0.5 mm/min. Tests at elevated temperatures were performed in argon. The 10-min dwell to equalize temperature and prevent shock-related behavior was used. Such details are described elsewhere [22].

Hardness was determined by an MMT-7 Vickers hardness tester (Matsuzawa MMT-7; Matsuzawa SEIKI Co., Ltd., Tokyo, Japan) using a load of 9.8 N with a dwell time of 15 s following the standard procedure (ASTM C 1327–15).

3 Results and Discussion

Using X-ray diffraction, we analyzed the SPSed TTZ ceramic specimens and bars following high-temperature flexural tests. After the SPS consolidation, a single-phase ceramic with the lattice parameter a = 4.4583 Å was identified. This remained unchanged for specimens tested at 1000 °C or 1600 °C. However, after the flexural tests at 1800 °C, we noticed the appearance of additional phases. For these specimens, the refinement results can be summarized as follows: the main phase with the lattice parameter a = 4.458(3) Å occupied over 54 vol.%, while

two other phases roughly contributed 37 and 8 vol.%. The lattice parameter for these phases was evaluated as a = 4.436(9) Å, and a = 4.493(7) Å. The refinement results are summarized in **Table 1**.

In conjunction with the XRD analysis (**Figure 1**), an SEM investigation of the fractured surfaces after flexural tests (**Figures 2,3**) confirmed the existence of at least three phases after the flexural tests at 1800 °C (**Figure 3**). The fourth phase was found to be free carbon which occupied less than 1 vol% based on the ImageJ analysis. The EDX results suggested that it is possible to estimate that at least 61 vol.% of the examined grains had an equimolar ratio between the Ti, Ta and Zr atoms; 29 vol.% were occupied by the phase with a higher contribution of Ta (Ta, 21–23 mol.%), while roughly 9 vol.% was occupied by the Ti-rich phase (Ti, 19–21 mol.%). This information was used to assign phases resulting from the refinement (see **Table 1**). The theoretical density of the TTZ bulk was estimated to be 7.617 g/cm^3, while the true density measured using the water immersion technique was 7.573 g/cm^3.

The application of the EDX methods allowed us to observe the local chemical gradient in the metal atoms which becomes quite evident while examining the specimen deformed at 1800 °C (**Fig. 3**). Overall, this may satisfy both the observations [15–17] and the high-entropy alloy concept [7] in which local order–disorder peculiarities may control the macroscopic properties.

It can be suggested that the appearance of these local gradients is due to the different diffusion rates for metal and carbon atoms in the pure metals or carbides

[4]. According to the analysis by Andrievsky [4], the difference in diffusivities becomes rate controlling above 0.7 Tmelting (i.e., >2100 °C), thus at lower temperatures the solubility limit [15–17] is rate controlling.

Furthermore, in general, binary systems of group IV and V metal carbides will may have a two-phase region below 2000 °C, and the addition of the WC or VC carbides will expand this multi-phase region [18]. Thus, the observed quasi-decomposition of the solid-solution carbide into several different phases can be considered as a 'low-temperature' peculiarity. A previous study [12] suggested that at 1700 °C, the pseudo-ternary TiC–ZrC–HfC system had a clear two-phase region. These were explained by the low solubility of ZrC and HfC in TiC. Meanwhile ref. [15] confirmed that for the TiC–ZrC system at 1300 °C, the decomposition of the solid-solution will take place following a long-term annealing. In this respect, the layer-by-layer oxidation behavior of the high-entropy ceramics [19] may be triggered by a similar driving force, i.e., low solubility or different diffusivities.

3.1 Mechanical properties

The average hardness lies within the range of 24.4±1.2 GPa. The measured values in the present work were on the same level with the values reported for high-entropy carbides with four and five transition metal atoms (**Table 2**) [2,8,11–14,24–28]. Vickers hardness values can be strongly affected by residual porosity or grain size [29]. Hardness of monolithic titanium carbide reported in ref. [27]

serves as an example. Hence, it is difficult to speculate if solid-solution hardening affected hardness of ternary carbide in the present study. Such conclusion can be postulated based on results on the monolithic carbides [30] and binary carbides [2,25,26].

Data of the temperature dependence for the strength of the individual monolithic TaC, TiC, and ZrC carbides are summarized in **Figure 4** [31–37]. Within these monolithic UHTCs, titanium carbide [33,34] has a slight variation in strength before 1400–1500 °C (brittle to ductile transition temperature, BDTT), followed by a rapid strength decrease due to activation of the macroscopic plastic deformation [38]. A similar trend can be observed for tantalum carbide in ref. [38]. The tendencies for ZrC are fully summarized in ref. [2]. For the monolithic zirconium carbide ceramics [2,35,39], the transition between the brittle and ductile fracture is associated with a clear maximum. The peak strength for these ceramics is usually observed in the vicinity of the BDTT, but the position of the peak is quite sensitive to (a) grain size and (b) consolidation conditions, i.e., a higher consolidation temperature allows shifting the peak strength to the higher temperatures.

The flexural strength data of the binary or ternary carbides are limited by [36] and [8]. In [36], the NbC–ZrC solid-solution follows a trend similar to the individual NbC or ZrC. While the data for the ternary high-entropy carbide (Ta,Zr,Nb)C suggested that the behavior of the ternary ceramic is comparable to

the data for the monolithic NbC [31,32] or NbC–ZrC [36] solid-solution, it also suggests that the magnitude for the solid-solution strengthening contribution.

The lattice strain accumulated during the SPS consolidation may cause high strength at room temperature (700 MPa) for the $(Ta_{1/3}Ti_{1/3}Zr_{1/3})C$ carbide. The decrease in strength noticeable at 1000 °C can be explained as the effect of the reheating [21] to higher temperatures, where the accumulated thermal stresses should relax. At 1600 °C or 1800 °C, the flexural strength remained unchanged within 300±25 MPa, which is not typical for other monolithic carbides in this temperature region.

3.2 High-temperature toughness

The high-temperature fracture toughness data for monolithic UHTC carbides were not previously reported, while at room temperature, TaC has a toughness between 3 and 4 MPa $m^{1/2}$ [40], and below 3 MPa $m^{1/2}$ [4,41] for the monolithic TiC or ZrC using the indentation method. The room temperature toughness data of the TTZ high-entropy ceramic favorably agreed with the data for the monolithic carbides (3.2 MPa $m^{1/2}$) [14].

Despite the fact that reheating above 1000 °C causes a decrease in strength, the toughness remains unchanged at 1000 °C, and rises to 3.4 MPa $m^{1/2}$ at 1600 °C. Interestingly, despite an elastic loading behavior at 1800 °C the fracture toughness increases up to 4.4 MPa $m^{1/2}$. In the absence of the toughness data for these temperatures, we can speculate that the local ‘decomposition’ of carbide

into several carbide phases observed in (**Fig. 3**) may contribute to the increase in toughness. To confirm our observation, an additional K_{IC} test was performed at 1800 °C. During this test the specimen was immediately loaded after 1800 °C was reached (10-min dwell was used otherwise). It resulted in the fracture toughness of 2.9 MPa $m^{1/2}$, but essentially, a local chemical gradient was not observed using EDX (see inset, **Figure 5**). The toughness value itself could not be fully understood as it is believed that thermal shock may contribute to the decrease in the toughness [2, 4].

Although one expects the sufficient contribution of plastic deformation at 1800 °C, neither of the loading curves recorded within this study had a visible plastic part. Thus, it is thought that an ~30% increase in toughness cannot be fully explained by contribution of the local plastic deformation [38]. For the ZrB_2–ZrC ceramics the increase in toughness coincided with the increase in strength at the elevated temperatures [42] attributable to blunting of the crack tip due to plastic flow.

For the TTZ ceramics, the fracture stress remained essentially constant from 1000 °C to 1600 °C, suggesting the absence of crack tip blunting. Furthermore, at the temperatures of 1000 °C and higher, from the observation of fracture surface a subcritical crack growth is considered to occur. The extent of slow crack growth increases with increasing temperature and is intergranular in nature (see **Table 1**).

Mechanistically, crack blunting can be expected as incipient crack-branching or slippage along the grain boundaries in proportion to the local resolved shear stress within the stress field of the crack tip. These agree with the crack propagation observed for the bars at 1800 °C (**Fig. 6**).

Figures 3,5, and **6** suggest that the local chemical gradient in TTZ carbide is only one of the factors that contribute to the fracture toughness increase, and its contribution is expected to be similar to that of the transformation induced toughening, i.e., via generation of the local microcracks. This is in agreement with observation in ref. [8] at elevated temperatures. Nevertheless, local decomposition was not observed in [8] for (Ta,Zr,Nb)C, suggesting that compounds with Ti and Zr may be affected [15–17], considering solubility of ZrC in TiC [17].

Furthermore, without reliable data on the coefficient of thermal expansion (CTE) or elastic moduli of the binary or ternary carbides it is not possible to make an estimation for toughness behavior using models proposed in [43,44]. For example, data on the CTE for HfC–TaC ceramic reported in [25, 45] had different trends: (i) monotonic growth following a rule of mixtures [25], (ii) a curve with a clear maximum for equimolar concentration but with low CTE for other non-equimolar [45]. Thus the estimation using a model proposed in [43] may lead to confusing results. Consider a precipitation process of the TaC from HfC–TaC, where a solid-solution carbide remains as a matrix. Using data of ref. [25] (**Table 3**) and assuming a 20 vol.% of the TaC precipitates, and with a 1800 °C

temperature difference one can estimate [43], that at room temperature matrix will under tensile stress of 52 MPa, while TaC will be under compressive stress of 208 MPa. If one assumes the that the size of the precipitates is 1 μm, the toughness of the 'composite' should decrease (i.e., positive ΔK_I) by 0.09 MPa $m^{1/2}$ (0.03 MPa $m^{1/2}$ for 100 nm, 0.31 MPa $m^{1/2}$ for 10 μm). This suggests that upon the reheating, ignoring the plasticity, toughness of the composite should increase by the same amount. Similar estimation can be made if a matrix is a 1:1 solid-solution, while precipitates are 4:1 and 1:4 solid-solutions (**Table 4**). **Figure 7** provides a visual illustration how the toughness would change for the solid-solution carbide if a solid-solution phase with (a) higher or (b) lower CTE compared with matrix is being precipitated during cooling. Any change in CTE ratio between newly precipitated phase, its volume or size may lead to enhancement of this effect. As underlined above, due to the absence of the CTE data on ternary (Ta,Ti,Zr)C it is unwise to bold predictions using approach described in [43]. **Figure 7** or **Table 4** clearly illustrate conditions for increase in toughness due to mismatch in thermal expansion for the multiphase carbide ceramics, nevertheless this scenario is valid for the matrix–inclusion configuration existing during cooling-heating or heating-cooling cycles, whereas we observe phases that form *in situ* at 1800 °C.

Analysis of ref. [44] suggests that the fracture toughness should decrease with the increase in temperature based on the decay of elastic modulus. Using data in **Fig.**

4 as a source for a first approximation, one should expect a 20% decrease in toughness at 1800 °C, but the opposite observation was made.

This suggests that further work involving, for example, evaluation of the thermal expansion for solid-solution carbides and their elastic moduli at elevated temperatures, which are beyond scope of this work, is needed to clarify details on high-temperature toughening in ultra high temperature carbides.

The observation of the crack propagation on the bar surface after 1800 °C suggests that additional mechanisms can be involved, such as crack branching and crack deflection, which are among the mechanisms involved in the high-temperature fracture. The latter observations may suggest contribution of the crack blunting via plasticity, as it was observed in [46]. Overall, the observed decomposition process and data in refs. [15–17] at lower temperatures indicate that this process can be tailored, if required. However, the exact temperature range for this *de facto* self-toughening phenomenon cannot be currently predicted as further experimental confirmation is required.

Conclusions

Bulk solid-solution high-entropy carbide ceramics have been obtained using the spark plasma sintering method. Phase analysis via lattice parameter measurements by X-ray diffraction showed that after subsequent flexural or fracture toughness tests at 1800 °C, the (Ta,Ti,Zr) carbide undergoes local decomposition and changes to the three-phase ceramic.

High-temperature fracture toughness for these compounds was reported for the first time. It was noted that the toughness remains unchanged up to 1600 °C. During the tests at 1800 °C, the fracture toughness reaches 4.4 MPa $m^{1/2}$. The increase in the fracture toughness can be attributed to the observed local carbide decomposition, however, a fracture analysis suggests that multiple mechanisms may also contribute to the improvement.

Acknowledgements

D.D. was supported by World Premier International Research Center Initiative (WPI), MEXT, Japan.

References

[1] Fahrenholtz WG, Wuchina EJ, Lee WE, et al., editor. Ultra-high temperature ceramics. Hoboken (NJ): Wiley; 2014.

[2] Zubarev PV High-temperature strength of the interstitial phases. Moscow (USSR): Metallurgiya; 1985, [in Russian].

[3] Mroz C. Processing TiZrC and TiZrB2. *Am Ceram Soc Bull.* 1994;**73**:78–81.

[4] Andrievski RA, Spivak II. Strength of Refractory Compounds. Chelyabinsk (USSR): Metallurgiya; 1989 [in Russian].

[5] Oses C, Toher C, Curtarolo S. High-entropy ceramics. *Nat Rev Mater.* 2020;**5**:295–309.

[6] Castle E, Csanadi T, Grasso S, et al. Processing and Properties of High-Entropy Ultra-High Temperature Carbides. *Sci Rep.* 2018;**8**:8609.

[7] Sarker P, Harrington T, Toher C, et al. High-entropy High-Hardness Metal Carbides Discovered by Entropy Descriptors. *Nat Commun.* 2018;**9**:4980.

[8] Demirskyi D, Borodianska H, Suzuki TS, et al. High-temperature flexural strength performance of ternary high-entropy carbide consolidated via spark plasma sintering of TaC, ZrC and NbC. *Scr Mater.* 2019;**164**:12–16.

[9] Wei X-F, Liu J-X, Li F, et al. High entropy carbide ceramics from different starting materials. *J Eur Ceram Soc.* 2019;**39**[10]: 2989–94.

[10] Wang K, Chen L, Xu C, et al. Microstructure and mechanical properties of (TiZrNbTaMo)C high-entropy ceramic. *J Mater Sci Technol.* 2020;**39**[15]:99–105.

[11] Sedegov A, Vorotilo S, Tsybulin V, et al. Synthesis and study of high-entropy ceramics based on the carbides of refractory metals. *IOP Conf Series: Materials Science and Engineering*. 2019;**558**:012043. https://dx.doi.org/10.1088/1757-899X/558/1/012043.

[12] Feng L, Fahrenholtz WG, Hilmas GE. Low- temperature sintering of single- phase, high- entropy carbide ceramics. *J Am Ceram Soc.* 2019;**102**:7217–7224.

[13] Yan XL, Contantin L, Lu YF, et al., (Hf0.2Zr0.2Ta0.2Nb0.2Ti0.2)C high-entropy ceramics with low thermal conductivity. *J Am Ceram Soc.* 2018;**101**:4486–4491.

[14] Ye BL, Wen TQ, Huang KH, et al. First- principles study, fabrication, and characterization of (Hf0.2Zr0.2Ta0.2Nb0.2Ti0.2)C high- entropy ceramic. *J Am Ceram Soc.* 2019;**102**:4344–4352.

[15] Borgh I, Hedström P, Blomqvist A, et al. Synthesis and phase separation of (Ti,Zr)C. *Acta Mater.* 2014;**66**:209–218.

[16] Li Y, Katsui H, Goto T. Microstructure evolution of (Ti,Zr)C solid solution at the initial stage of phase decomposition. *Materials Today: Proceedings.* 2017;**4**:11449–11512.

[17] Murray P, Weston JE. The 1700 °C isothermal section of the pseudoternary system TiC-ZrC-HfC. *J Less Common Met.* 1981;**81**:173–179.

[18] Kieffer R., Benesovsky F. Hartstoffe, Wien: Springer; 1963 [in German].

[19] Ye B, Wen T, Liu D, et al. Oxidation behavior of (Hf0.2Zr0.2Ta0.2Nb0.2Ti0.2)C high-entropy ceramics at 1073-1473 K in air. *Corros Sci.* 2019;**153**:327–332.

[20] Cullity BD. Elements of X-Ray Diffraction. 2nd ed. Reading (MA): Addison-Wesley Publishing Inc; 1978.

[21] Demirskyi D, Vasylkiv O. Analysis of the high-temperature flexural strength behavior of B4C–TaB2 eutectic composites produced by in situ spark plasma sintering. *Mater Sci Eng A.* 2017;**697**:71–78.

[22] Demirskyi D, Solodkyi I, Nishimura T, et al. High- temperature strength and plastic deformation behavior of niobium diboride consolidated by spark plasma sintering. *J Am Ceram Soc.* 2017;**100**:5295–5305.

[23] Demirskyi D, Vaslykiv O. Spark plasma sintering and high-temperature strength of B6O–TaB2 ceramics. *J Eur Ceram Soc.* 2017;**37**[8]:3009–3014.

[24] Sciti D, Guicciardi S, Nygren M. Densification and mechanical behavior of HfC and HfB2 fabricated by spark plasma sintering. *J Am Ceram Soc.* 2008;**91**:1433–1440.

[25] Cedillos-Barraza O, Grasso S, Al Nasiri N, et al. Sintering behaviour, solid solution formation and characterisation of TaC, HfC and TaC–HfC fabricated by spark plasma sintering. *J Eur Ceram Soc.* 2016;**36**:1539–1548.

[26] Acicbe RB, Goller G. Densification behavior and mechanical properties of spark plasma- sintered ZrC–TiC and ZrC–TiC–CNT composites. *J Mater Sci.* 2013;**48**:2388–2393.

[27] Cheng L, Xie Z, Liu G, et al. Densification and mechanical properties of TiC by SPS- effects of holding time, sintering temperature and pressure condition. *J Eur Ceram Soc.* 2012;**32**:3399–33406.

[28] Demirskyi D, Sakka Y. High-temperature reaction consolidation of TaC–TiB2 ceramic composites by spark-plasma sintering. *J Eur Ceram Soc.* 2015;**35**:405–410.

[29] Rice RW. Mechanical Properties of Ceramics and Composites: Grain and Particle Effects. New York (NY): CRC Press; 2000.

[30] Gillman JJ Hardnesses of Carbides and Other Refractory Hard Metals. *J Appl Phys.* 1970;**41**(4):1664–1666.

[31] Ordan'yan SS, Stepanenko EK, Sokolov IV. Strength of NbC-NbB2 sintered composites. *Izv Vyssh Uchebn Zaved, Khim.* 1984;**27**[10]:1201–1203.

[32] Kelly A, Rowcliffe DJ. Deformation of polycrystalline transition metal carbides. *J Am Ceram Soc.* 1967;**50**:253–256.

[33] Katz AP, Lipsitt HA, Mah T, et al. Mechanical behaviour of polycrystalline TiC. *J Mater Sci.* 1983;**18**:1983–1992.

[34] Miracle DB, Lipsitt HA. Mechanical Properties of Fine- Grained Substoichiometric Titanium Carbide. *J Am Ceram Soc.* 1983;**66**[8]: 592–597.

[35] Zubarev PV, Kuraev AB. Stress relaxation in zirconium carbide. 2. Mechanisms of stress relaxation. The relationship of the processes of creep and relaxation. *Strength Mater.* 1994;**26**:132–136.

[36] Lanin AG, Zubarev PV, Vlasov KP. Mechanical and thermophysical properties of materials in HTGR fuel bundles. *Atomic Energy* 1993;**74**[1]:40–44.

[37] Demirskyi D, Nishimura T, Sakka Y, et al. High-strength TiB2–TaC ceramic composites prepared using reactive spark plasma consolidation. *Ceram Int.* 2016;**42**:1298–1306.

[38] Demirskyi D, Vasylkiv O. Mechanical properties of SiC–NbB2 eutectic composites by in situ spark plasma sintering. *Ceram Int.* 2016;**42**[16]:19372–19385.

[39] Zhao J, Zou J, Man Z-Y, et al. Dopant effects on high temperature mechanical properties of zirconium carbide ceramics. *Adv Appl Ceram* 2015;**114**(6):338–343.

[40] Silvestroni L, Pienti L, Guicciardi S, et al. Strength and toughness: the challenging case of TaC-based composites. *Composites B.* 2015;**72**:10–20.

[41] Maerky C, Guillou M-O, Henshall JL, et al. Indentation hardness and fracture toughness in single crystal TiC0.96. *Mater Sci Eng A.* 1996;**209**:329–336.

[42] Neuman EW, Hilmas GE, Fahrneholtz WG. Ultra- High Temperature Mechanical Properties of a Zirconium Diboride–Zirconium Carbide Ceramic. *J Am Ceram Soc.* 2016;**99**: 597–603.

[43] Taya M, Hayashi S, Kobayashi AS, et al. Toughening of a Particulate-Reinforced Ceramics-Matrix Composite by Thermal Residual Stress. *J Am Ceram Soc.* 1990;**73**[5]:1382–1391.

[44] Stewart RL, Bradt RC. Fracture of Polycrystalline MgAl2O4. *J Am Ceram Soc.* 1980;**63**[11–12]:619–623.

[45] Barantseva IG, Paderno VN. Thermal expansion of solid solutions in thesystems ZrC–NbC and HfC–TaC. in: Samsonov GV editor. Refractory Carbides. London (UK): Consultants Bureau; 1974, pp. 283–285.

[46] Maloy S, Heuer AH, Lewandowski J, et al. Carbon Addition to Molybdenum Disilicide: Improved High-Temperature Mechanical Properties. *J Am Ceram Soc.* 1991;**74**[10]:2704–2706.

Tables

Table 1 Summary of X-ray diffraction analysis and mechanical properties of TTZ ceramics

Temperature, °C	Lattice parameter, Å	Transgranular fracture, %	Strength, MPa	K_{IC}, MPa $m^{1/2}$
25	4.45833	>85	703±21	3.2; 3.2; 3.3
1000	4.45828	<14	322±16	3.2
1600	4.45829	<12	309±17	3.4
1800*	4.45836 (0.547) 4.43692 (0.369) 4.49373 (0.084)	<10	306±12	4.3; 4.5; 4.6
1800 [Y]	4.45829	<15	298±16	2.8

Notes:
* A clear multiphase ceramic was confirmed by EDX and XRD, numbers in brackets indicate the volume fraction.
[y] Immediate loading was used during the test.

Table 2 Hardness data on monolithic UHTC carbides and high-entropy carbides

Material	Grain size, μm	Load, N	Hardness, GPa	Reference
$(Ta_{1/3}Ti_{1/3}Zr_{1/3})C$	7.1±4.5	9.8	24.4±1.2	this study.
$(Ta_{1/5}Ti_{1/5}Zr_{1/5}\ Hf_{1/5}Nb_{1/5})C$	1–3	3	20.53	[11]
$(Ta_{1/5}Ti_{1/5}Zr_{1/5}\ Hf_{1/5}Nb_{1/5})C$	1.2±0.7	4.9	24.8±0.8	[12]
$(Ta_{1/5}Ti_{1/5}Zr_{1/5}\ Hf_{1/5}Nb_{1/5})C$	1.2±0.7	9.8	23±0.5	[12]
$(Ta_{1/5}Ti_{1/5}Zr_{1/5}\ Hf_{1/5}Nb_{1/5})C$	16.4±4.5	9.8	15	[13]
$(Ta_{1/5}Ti_{1/5}Zr_{1/5}\ Hf_{1/5}Nb_{1/5})C$	>10	9.8	22.5±0.3	[14]
$(Ta_{1/5}Ti_{1/5}Hf_{1/5}Nb_{1/5}\ Mo_{1/5})C$	1–3	3	22.62	[11]
TaC – HfC 50:50[X]	4.3±0.3	9.8	20.4±2.3	[25]
ZrC – TiC 80:20[Y]	<20	9.8	22.08±0.20	[26]
TiC – ZrC 50:50[X]	N.A.	4.9	21.78±1	[3]
TaC	5–10	9.8	14.7±3.2	[28]
TaC	5.8±0.2	9.8	13.9±0.7	[25]
TiC	4.59 ± 1.19**	9.8	29.10±2.41	[27]
TiC	N.A.	4.9	16.95±2	[3]
ZrC	N.A.	9.8	17.6±0.14	[26]
ZrC	N.A.	4.9	16.54±1	[3]
HfC	19±1	9.8	18.7±0.5	[24]
HfC	1.8±0.2	9.8	10.2±0.7*	[25]

Notes:
* not dense (85% of theoretical density);
** sample #8 was used;
X molar ratio was used;
Y volume ratio was used.

Table 3 Data on thermal expansion and Young moduli for TaC – HfC ceramic based on ref. [25]

Composition	Elastic modulus, E, GPa	Coefficient of thermal expansion (CTE), 10^{-6}, K^{-1}
TaC	458±6	7.08±0.33
4TaC–1HfC	459±5.8	7.24±0.53
1TaC–1HfC	539±11.2	7.41±0.28
1TaC–4HfC	438±17.8	7.59±0.3

Table 4 Evaluation of the thermal stresses and change in toughness for different matrix – inclusion configurations based on data of ref. [25]

Configuration		Average residual stress on matrix, MPa[Y,X]	Average residual stress on inclusion, MPa[Y]	ΔK_I,* change in fracture toughness after cooling to room temperature, MPa $m^{1/2}$
matrix	inclusion			
1TaC–1HfC	TaC	52	-208	0.09
1TaC–1HfC	4TaC–1HfC	26	-107	0.05
1TaC–1HfC	1TaC–4HfC	-28	111	-0.05

Notes:
[Y] cooling down to room temperature with a gradient 1800K;
[X] Upon cooling of the composite thermal stresses on the matrix and inclusion may has a negative value (phase is found to be in compression), while the positive value indicates that the phase is found to be in tension;
* assuming 1 μm inclusion side and its volumetric fractions of 20%; negative value of ΔK_I contributes to increase in fracture toughness;

Figure captions

Fig. 1. X-ray diffraction of the TTZ ceramic after SPS consolidation at 1973 °C and following the flexural strength test at 1800 °C. The inset shows refinement details for deformed specimen at 1800 °C for high-angle peaks. The bars indicate the allowed Bragg reflections for the *Fm-3m* structure. Observed lattice parameter as SPSed specimen a = 4.458 Å, deformed at 1800 °C: a = 4.4583(6) Å, a = 4.4369(2) Å, and a = 4.4937(3) Å (see **Table 1**).

Fig. 2. Fracture of the TTZ ceramic after flexural strength tests at (a,b) room temperature, (c,d) at 1000 °C, and (e,f) at 1600 °C. (a,c,e) images acquired using the SE mode, while (b,d,f) used the BSE mode.

Fig. 3. Fracture of the TTZ ceramic after fracture toughness test at 1800 °C using two different magnifications (×500, and ×2000). Areas of local carbide decomposition are marked with red (Ti) and green colors (Ta), equimolar TTZ carbide is colored with blue. Uncolored areas are due to EDX's depth limitation.

Fig. 4. Effect of temperature on the flexural strength of $(Ta_{1/3}Ti_{1/3}Zr_{1/3})C$ prepared in this study. (a) provides variation in strength for TTZ ceramic and for selected monolithic carbides [31–37]. The closed symbols indicate that the strength was measured using a four-point setup and the open symbols show the results of the three-point flexural strength tests. (b) shows typical loading curves for TTZ ceramics at 25 °C, 1000 °C and 1800 °C. Dashed lines in (b) visually show the Young's modulus evolution during the flexural tests at different temperatures.

Data for 1600 °C are not shown for clarity as they overlap with the data for 1000 °C.

Fig. 5. Fracture of the TTZ ceramic after flexural strength tests at 1800 °C using an immediate loading procedure. Insets show a linear mapping for Ta, Ti and Zr performed on the flat neighboring grains. Dotted lines show a tolerance limit for equimolar composition 16.6 at.% (assuming that C occupies 50 at.%).

Fig. 6. Possible toughening mechanism due to local chemical gradient at ambient temperature and at 1800 °C. Microcracks and related force fields are being generated as a result of the local carbide decomposition into several phases, initial high-entropy carbide acts as a matrix under residual compressive stresses. These microcracks may shield crack tip during fracture, or directly pin the crack. Note, that microcracks after the flexural strength tests at 2000 °C were observed in ref. [8]. Right image shows crack propagation behavior at the lateral surface of the test bar after fracture toughness test following three-point flexure at 1800 °C (SE mode).

Fig. 7. Change in fracture toughness during cooling (a,b) and (d,c) reheating using different relation in CTE between matrix and inclusion.

Figure 1

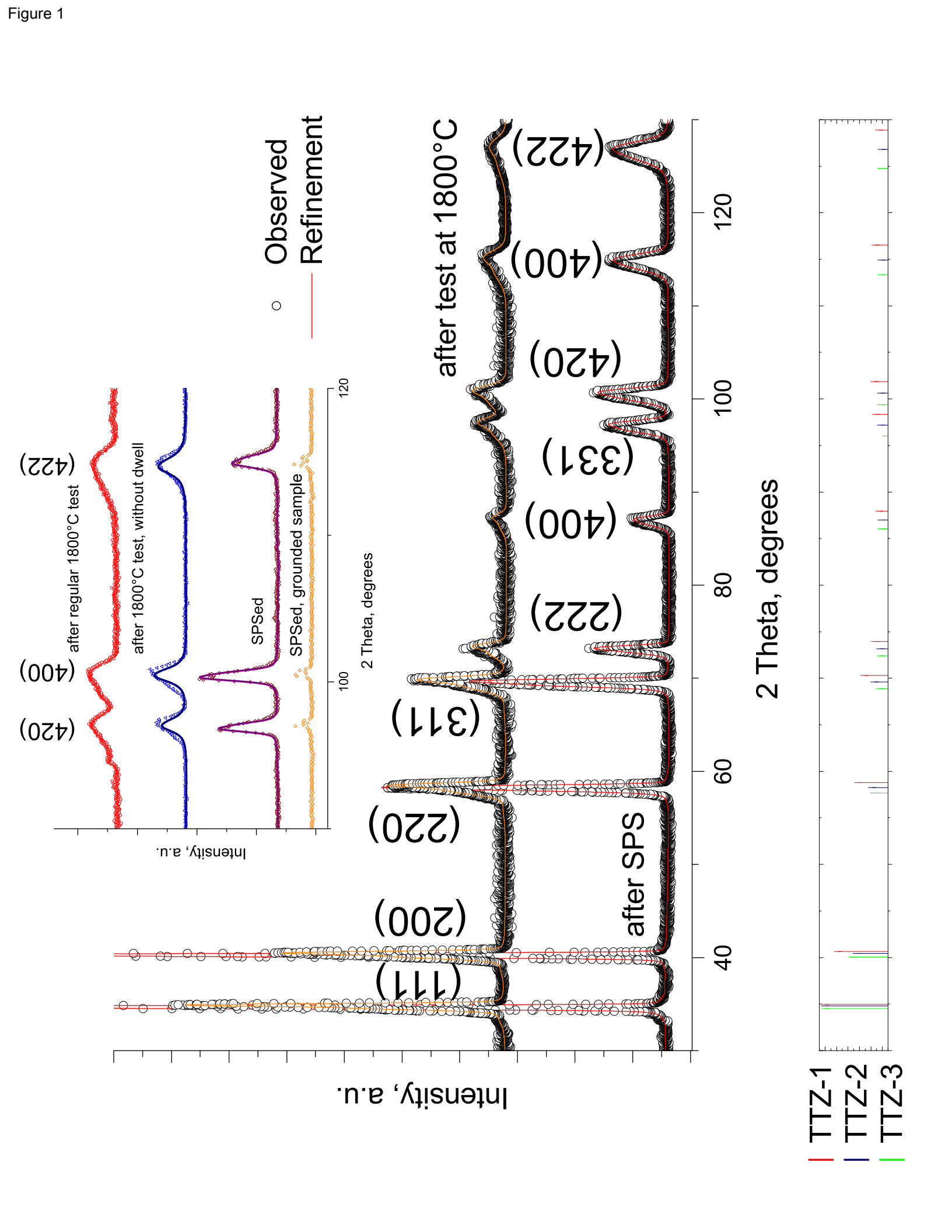
Intensity, a.u.
2 Theta, degrees
after SPS
after test at 1800°C
(111)
(200)
(220)
(311)
(222)
(400)
(331)
(420)
(400)
(422)
Observed
Refinement
SPSed
SPSed, grounded sample
after 1800°C test, without dwell
after regular 1800°C test
(420)
(400)
(422)
TTZ-1
TTZ-2
TTZ-3

Figure 2

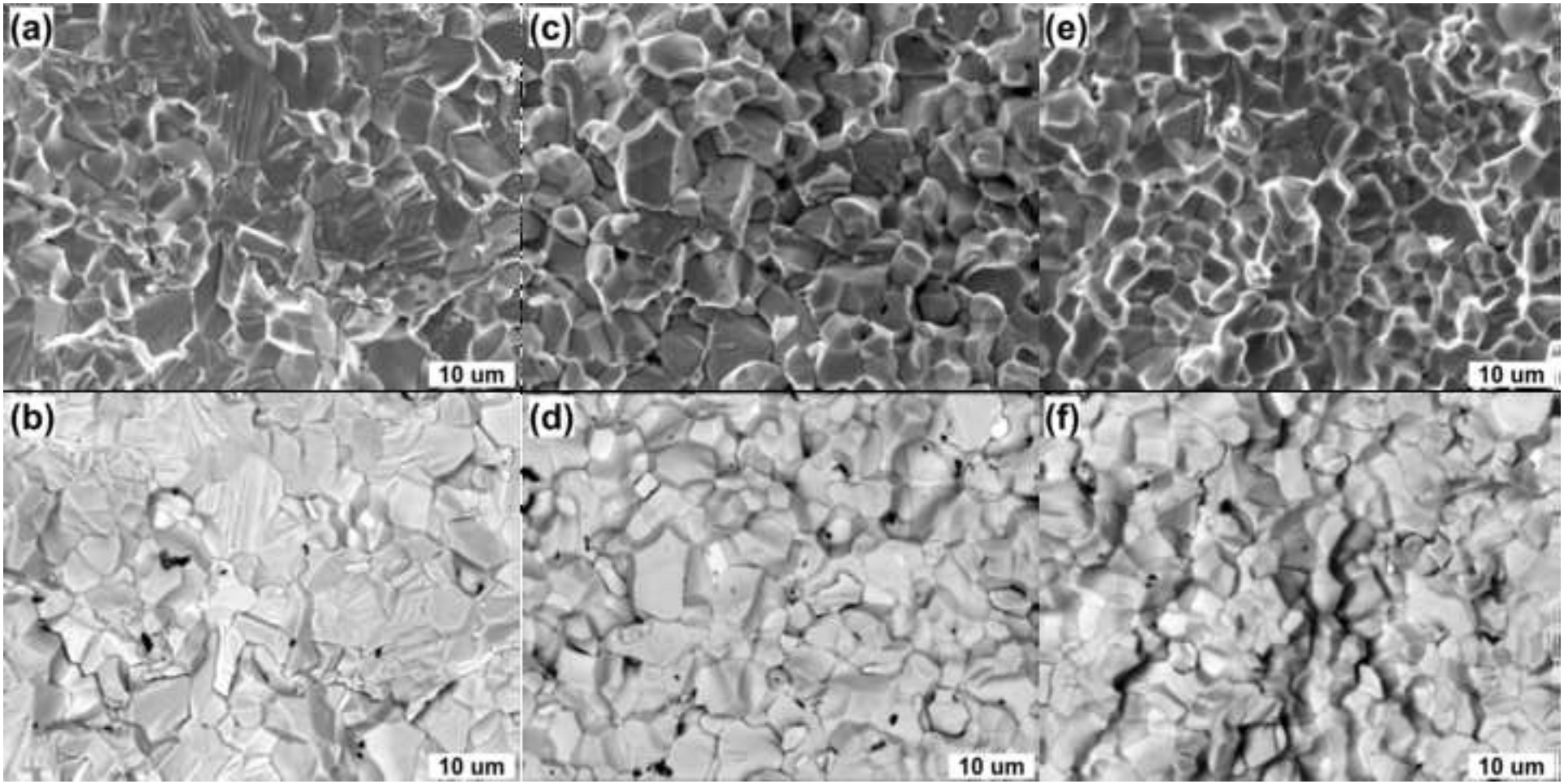

Figure 3

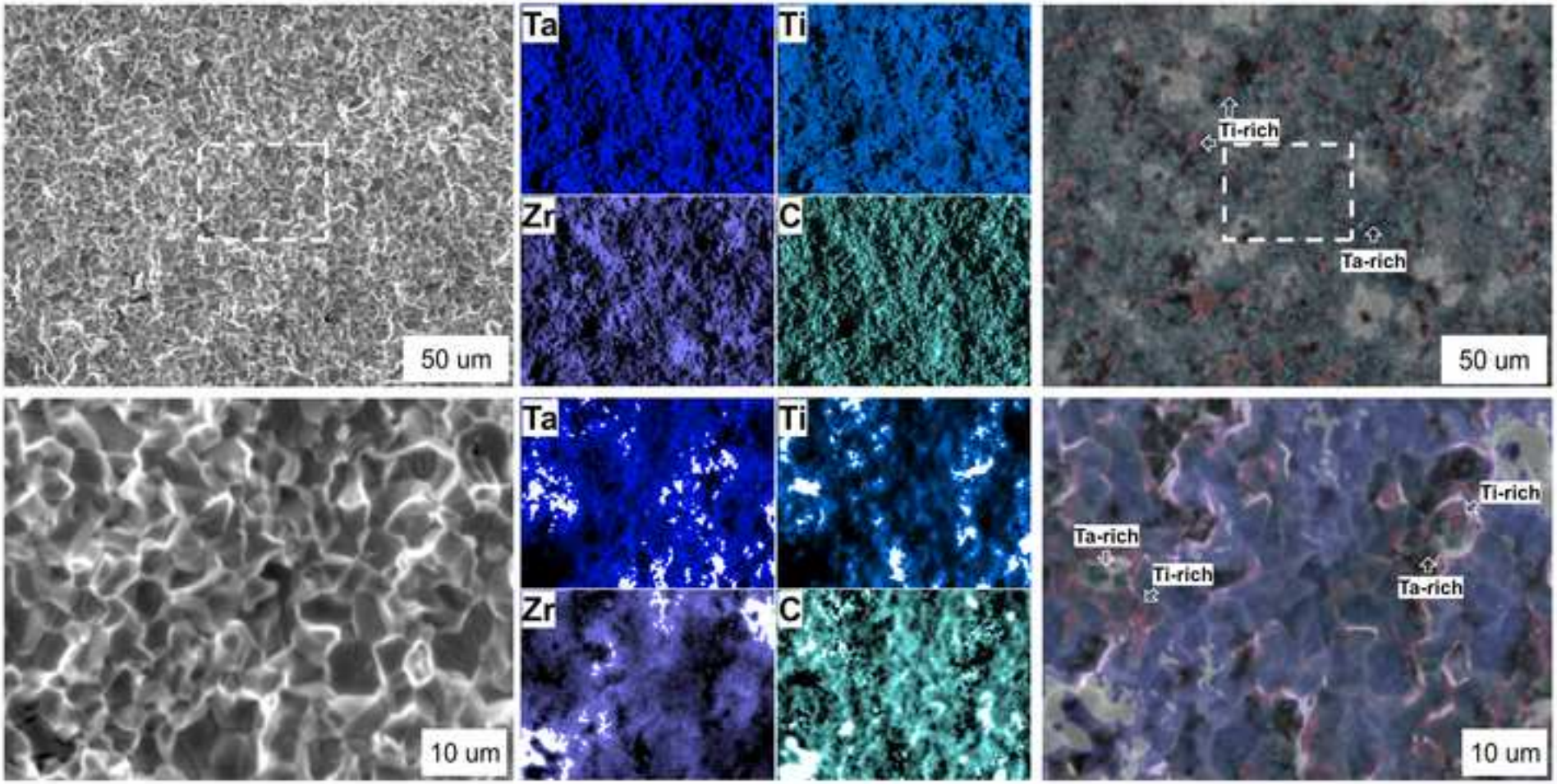
50 um
Ta
Ti
Zr
C
Ti-rich
Ta-rich
50 um
10 um
Ta
Ti
Zr
C
Ta-rich
Ti-rich
Ti-rich
Ta-rich
10 um

Figure 4

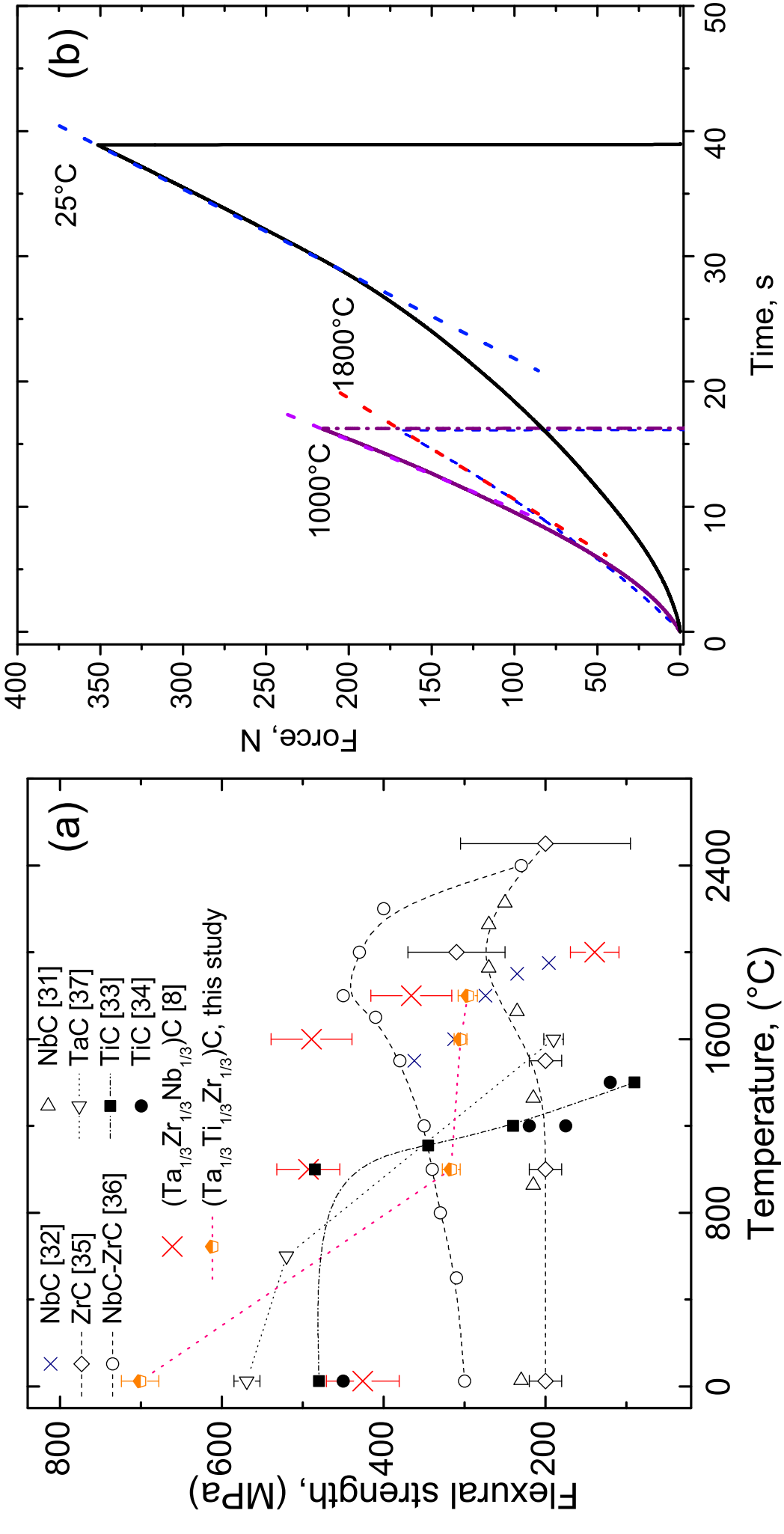
(a)
Flexural strength, (MPa)
Temperature, (°C)
NbC [32]
ZrC [35]
NbC-ZrC [36]
NbC [31]
TaC [37]
TiC [33]
TiC [34]
(Ta1/3Zr1/3Nb1/3)C [8]
(Ta1/3Ti1/3Zr1/3)C, this study
(b)
Force, N
Time, s
25°C
1800°C
1000°C

Figure 5

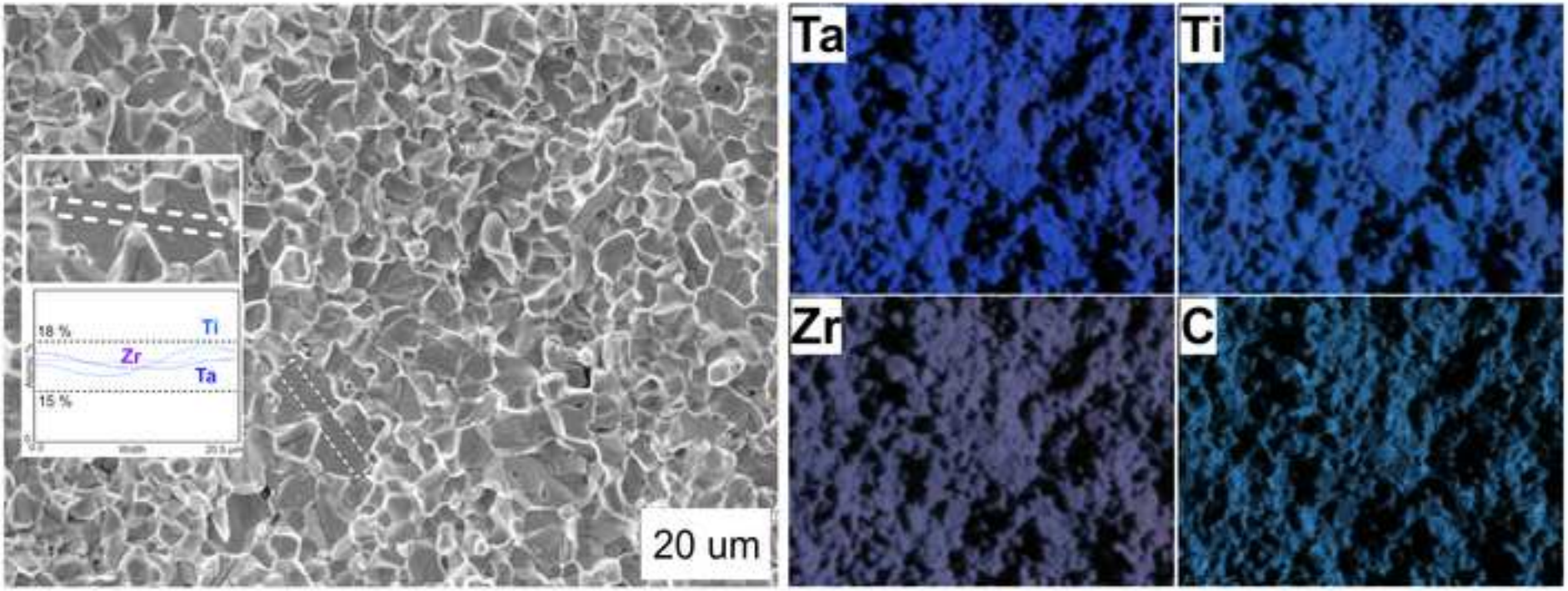

Figure 6

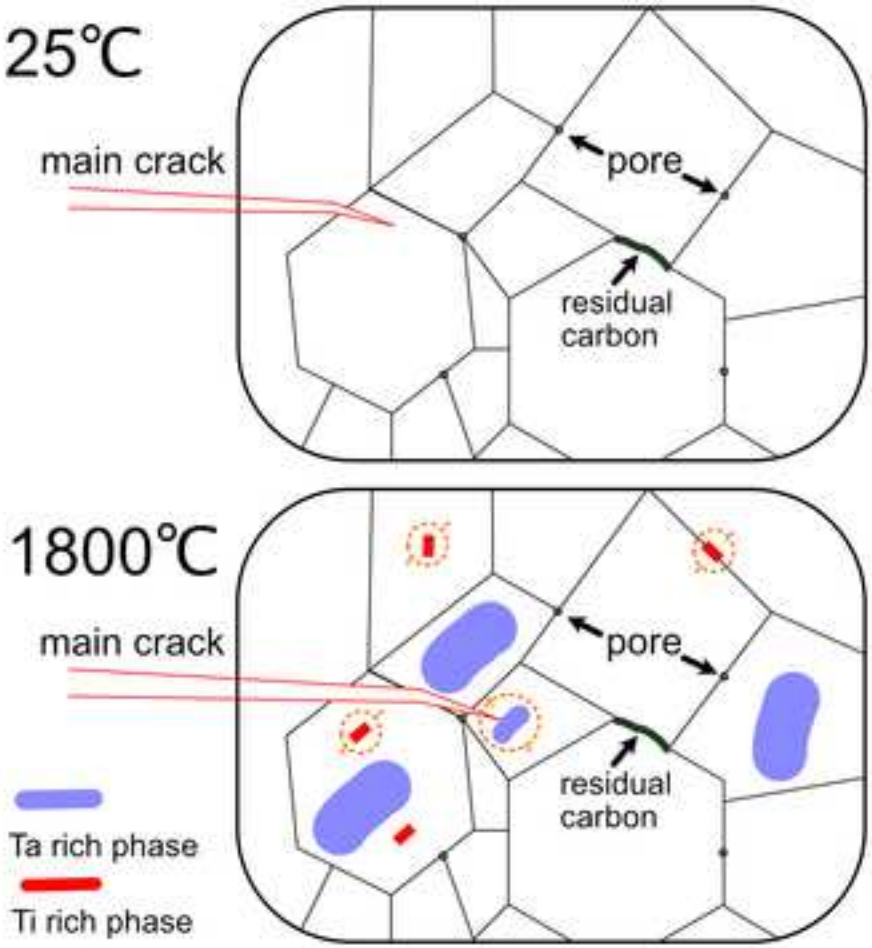
25℃
main crack
pore
residual carbon
1800℃
main crack
pore
residual carbon
Ta rich phase
Ti rich phase

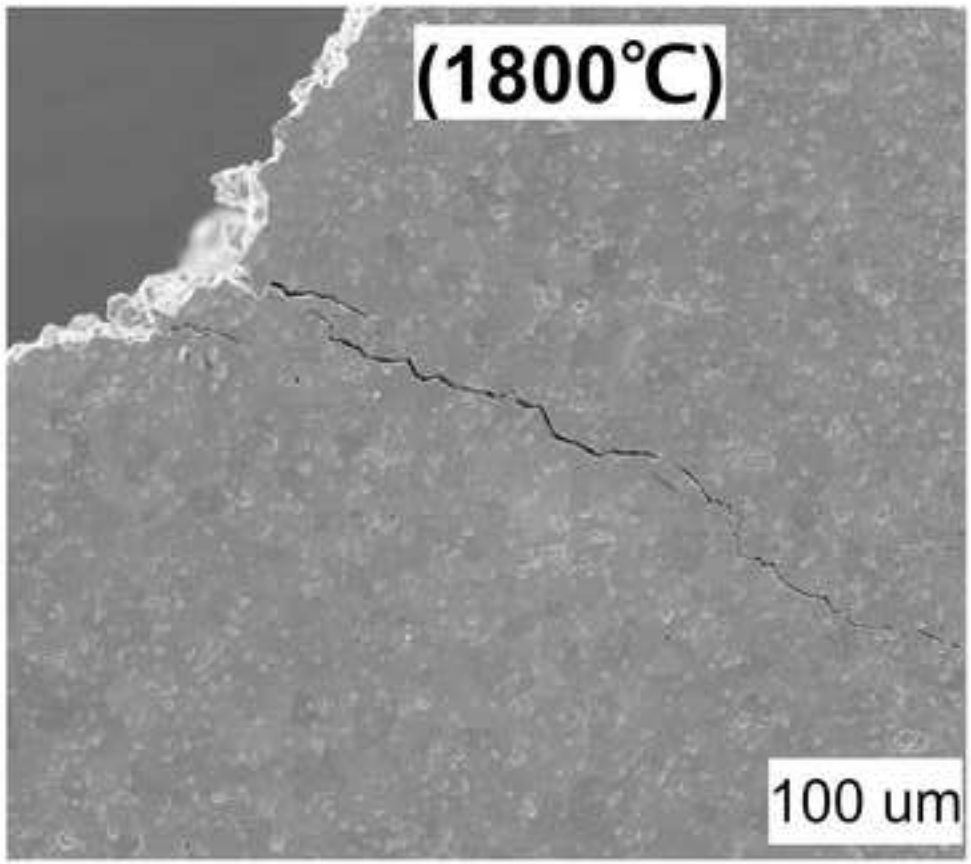
(1800℃)
100 um

Figure 7

(a)

Thermal expansion of inclusion > matrix

Inclusion will be under tensile stress

1800℃=>25℃

Effect
increase in K_{IC} at room temperature

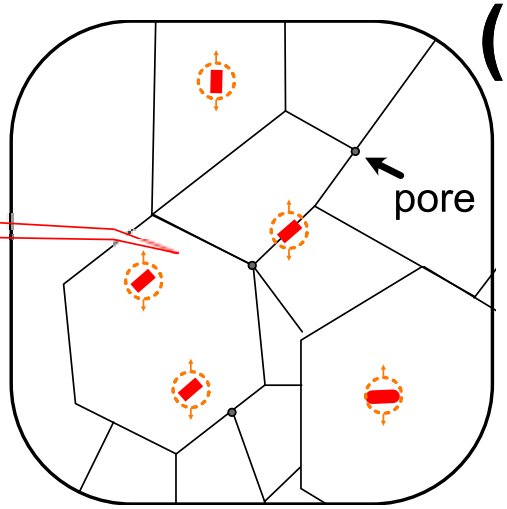

(b)

Thermal expansion of inclusion < matrix

Inclusion will be under compressive stress

1800℃=>25℃

Effect
decrease in K_{IC} at room temperature

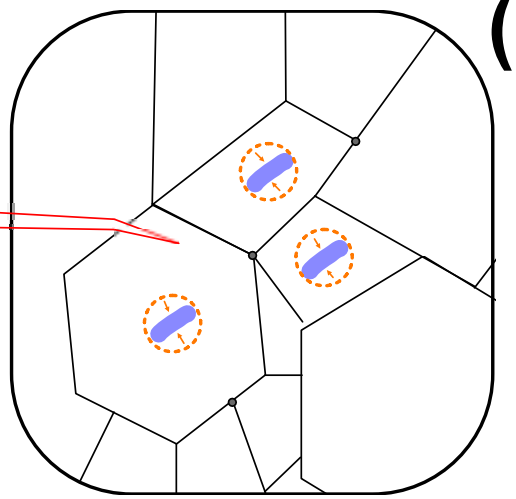

(c)

Inclusion will be under compressive stress during reheating

25℃=>1800℃

Effect
decrease in K_{IC}

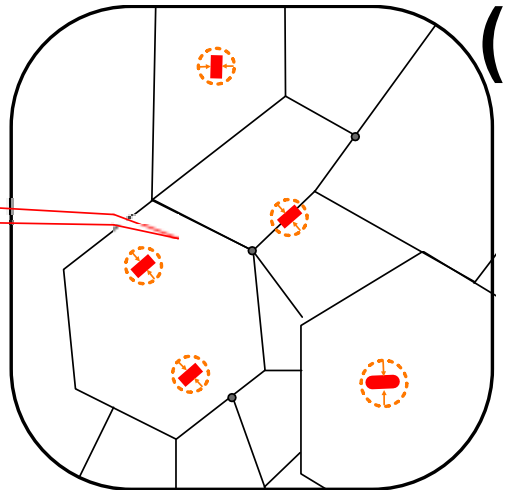

(d)

Inclusion will be under tensile stress during reheating

25℃=>1800℃

Effect
increase in K_{IC}

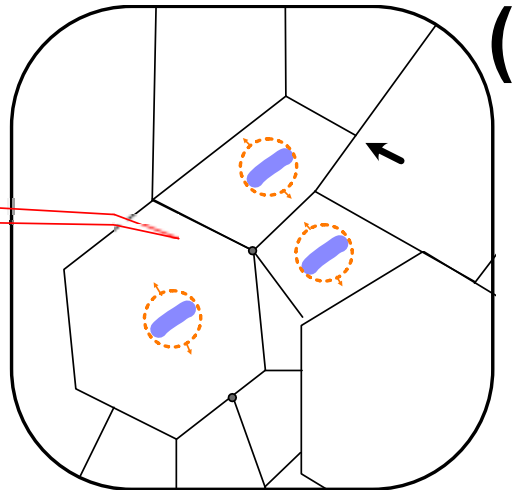

Supplementary Information for

High-temperature toughening in ternary high-entropy $(Ta_{1/3}Ti_{1/3}Zr_{1/3})C$ carbide consolidated using spark-plasma sintering

D. Demirskyi (a,b,c)†, T. Nishimura (b), T.S. Suzuki (b), Y. Sakka (b), O. Vasylkiv (b)†, and K. Yoshimi (c).

(a) WPI-Advanced Institute for Materials Research (WPI-AIMR), Tohoku University, 2-1-1 Katahira, Aoba-ku, Sendai, 980-8577 Japan
(b) National Institute for Materials Science, 1-2-1 Sengen, Tsukuba, Ibaraki 305-0047, Japan
(c) Department of Materials Science and Engineering, Tohoku University, 6-6-02 Aramaki Aza Aoba, Sendai, 980-8579, Japan

† Authors to whom correspondence should be addressed, Dmytro Demirskyi, demirskyi.dmytro.e2@tohoku.ac.jp, Oleg Vasylkiv oleg.vasylkiv@nims.go.jp

Details on diffusivities for UHTC carbides

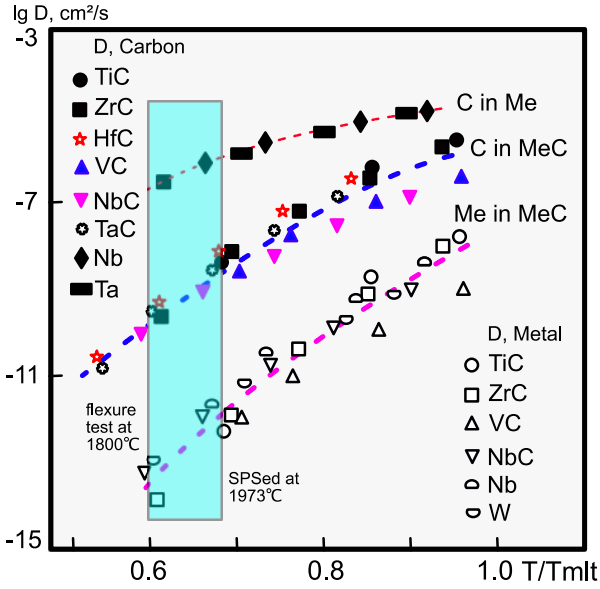

Fig. S1. Summary of the diffusivities of the transition metals, carbon in metals and carbides after Andrievsky [1]. Highlighted area lies between the highest temperature used for the tests (1800 °C) and the consolidation temperature (1973 °C).

Details on raw powders

Table S1 Characteristics of starting powders for the SPSed $(Ta_{1/3}Ti_{1/3}Zr_{1/3})C$.

Powder	Lot#	Particle size, µm	Impurities*, wt.%
TaC, Wako	LKP4101	0.7–2.1	Hf 0.15; Nb 0.05; O 1.00.
TiC, Wako	DCH6094	1–2	Al 0.15; O 0.41.
ZrC, Alfa Aesar	X24D058	0.5–2	Hf 0.80; O 0.74.

Determined by X-ray fluorescence, O determined by LECO, or provided by manufacturer.

Details on the refinement

Figure S2 shows refinement results obtained via TOPAS, while the **Figure S3** shows refinement performed using Profex [2]. Both refinement were performed using lattice parameter and CIF files obtained during initial refinement using TOPAS or GSAS-2 [3] (see **Figure S4**). Details on the statistical variation of lattice parameters are provided in **Tables S2–S4**.

Difference in metal occupancy atoms in the *Fm-3m* cell for TTZ1, TTZ2 and TTZ3 phases is visualized in **Figure S5**.

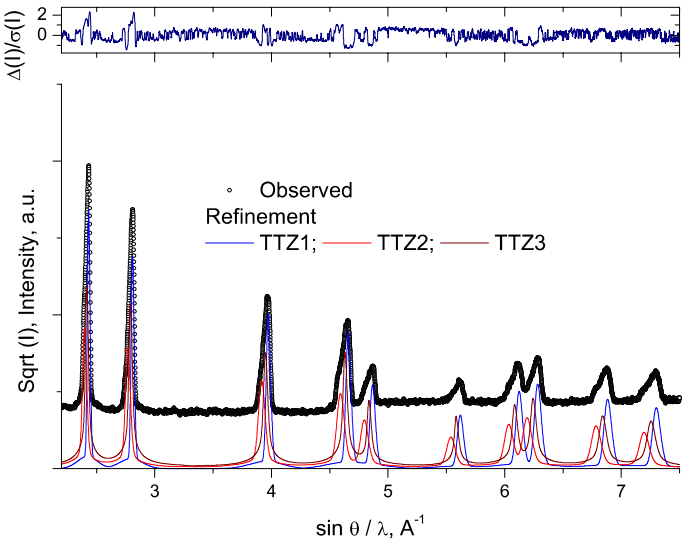

Fig. S2. Observed and calculated X-ray powder diffraction patterns (λ= 1.7902 Å) of the $(Ta_{1/3}Ti_{1/3}Zr_{1/3})C$ specimen following the 1800 °C test using TOPAS. Rwp: 8.56 %.

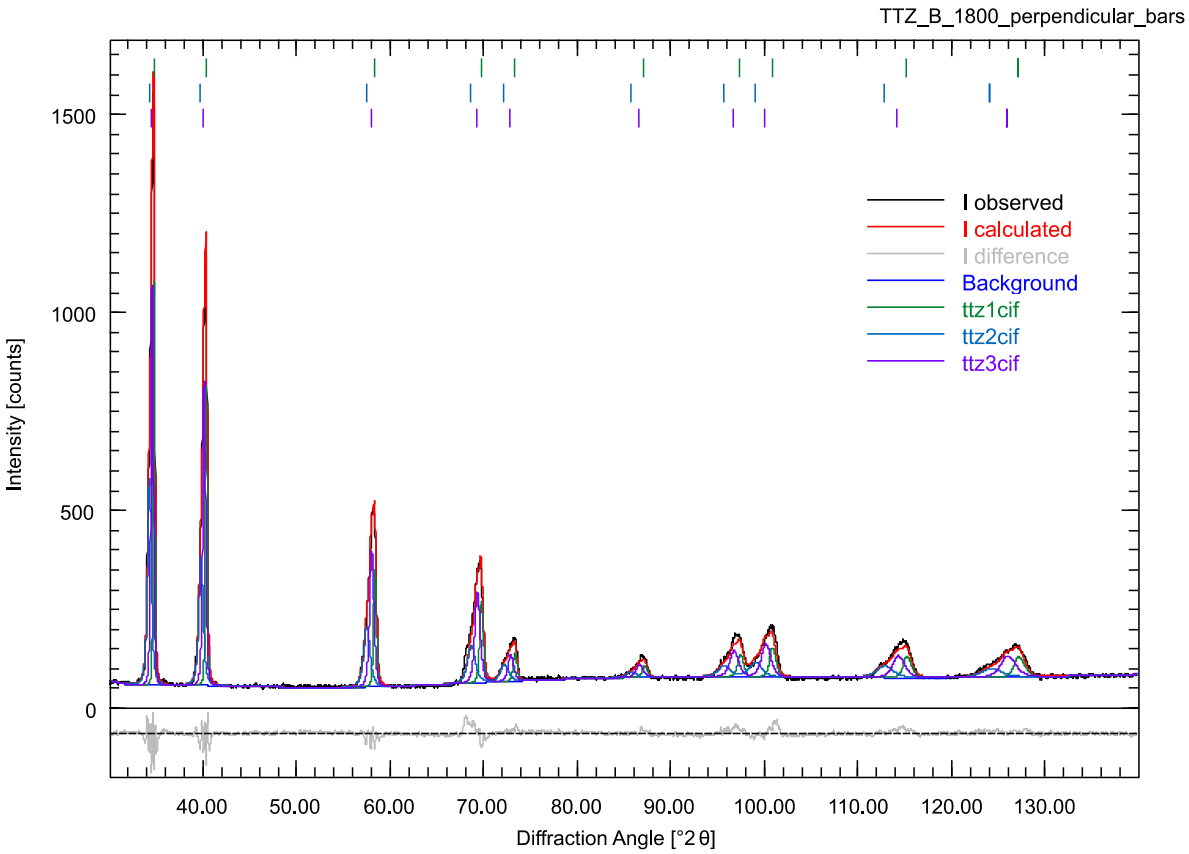

Fig. S3. Observed and calculated X-ray powder diffraction patterns (λ= 1.54060 Å) of the $(Ta_{1/3}Ti_{1/3}Zr_{1/3})C$ specimen following the 1800 °C test. Vertical ticks denote the Bragg positions. Rwp: 6.69 %.

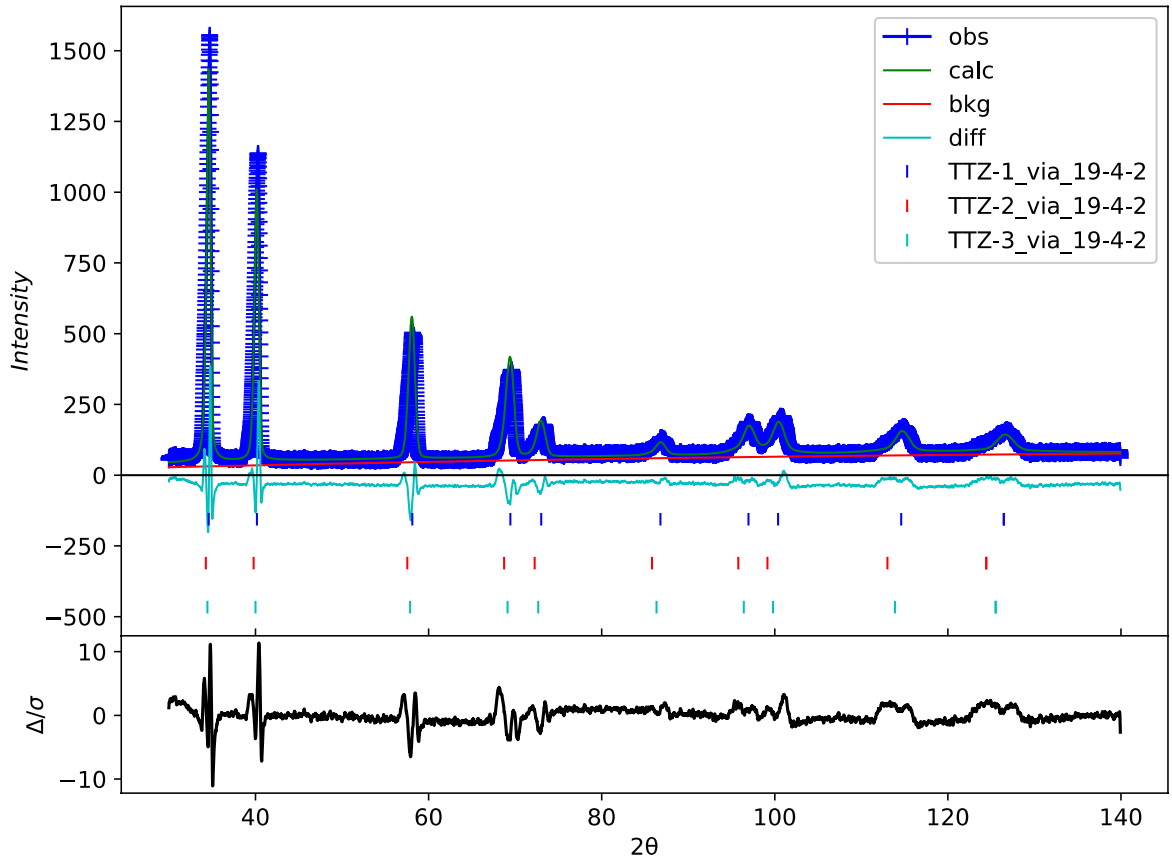

Fig. S4. An initial refinement performed to determine and optimize lattice parameters of the phases for $(Ta_{1/3}Ti_{1/3}Zr_{1/3})C$ specimen following the 1800 °C test using GSAS-2 [3]. Rwp: 14.0 %,. λ= 1.54060 Å. Vertical ticks denote the Bragg positions.

Table S2 Fivefold results of Rietveld refinement for the main phase in $(Ta_{1/3}Ti_{1/3}Zr_{1/3})C$ specimen following the 1800 °C test (for reproducibility estimation).

	Angular interval at Rietveld refinement, 2 theta					
	30-130			30-80		
TTZ1	a, Å	d,nm	vol., a.u.	a, Å	d,nm	vol., a.u.
1	4.45836	9044	0.546	4.45832	9101	0.563
2	4.45836	9015	0.545	4.45836	9080	0.558
3	4.45835	9064	0.548	4.45834	9024	0.559
4	4.45832	9041	0.547	4.45837	9102	0.542
5	4.45838	9047	0.547	4.45836	9049	0.546

median	4.45836	9044	0.547	4.45836	9080	0.558
st dev	0.00002	18	0.0011	0.00002	34	0.0091

Table S3 Fivefold results of Rietveld refinement for the second phase in $(Ta_{1/3}Ti_{1/3}Zr_{1/3})C$ specimen following the 1800 °C test (for reproducibility estimation).

	Angular interval at Rietveld refinement, 2 theta					
	30-130			30-80		
TTZ-2	a, Å	d,nm	vol., a.u.	a, Å	d,nm	vol., a.u.
1	4.43692	2740	0.368	4.43693	2750	0.372
2	4.43694	2752	0.374	4.43692	2810	0.379
3	4.43691	2739	0.371	4.43693	2789	0.375
4	4.43693	2737	0.369	4.43694	2801	0.372
5	4.43691	2755	0.369	4.43691	2755	0.381
median	4.43692	2740	0.369	4.43693	2789	0.375
st dev	0.00001	8	0.0024	0.00001	27	0.0041

Table S3 Fivefold results of Rietveld refinement for the second phase in $(Ta_{1/3}Ti_{1/3}Zr_{1/3})C$ specimen following the 1800 °C test (for reproducibility estimation).

	Angular interval at Rietveld refinement, 2 theta					
	30-130			30-80		
TTZ-3	a, Å	d,nm	vol., a.u.	a, Å	d,nm	vol., a.u.
1	4.49375	1092	0.086	4.49373	1088	0.065
2	4.49374	1089	0.081	4.49374	1089	0.063
3	4.49372	1075	0.081	4.49373	1087	0.066
4	4.49373	1088	0.084	4.49374	1089	0.086
5	4.49373	1086	0.084	4.49373	1088	0.073
median	4.49373	1088	0.084	4.49373	1088	0.066
st dev	0.00001	7	0.0022	0.00001	1	0.0094

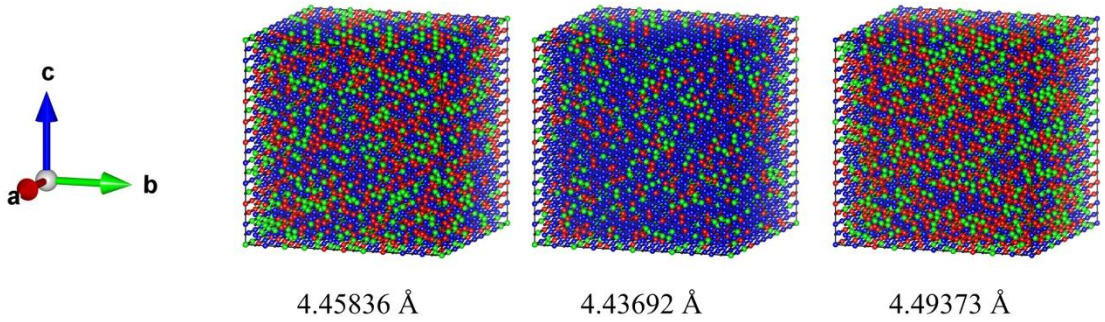

Fig. S5. Visual representation of high-entropy carbide phases derived during Rietveld refinement of the bar after flexural test at 1800 °C test using a 10x10x10 supercell (Ta – red, Ti – blue, Zr – green, C – black). Phase with mean lattice parameter a = 4.4583(6) Å was main phase in all observed specimens.

Thermal expansion in binary solid-solution of transition metal carbides

Figures S6–S9 show selected data on thermal expansion coefficients of binary carbides [4–6]. For this purpose we selected three studies where coefficient of thermal expansion (CTE) was determined for specimens consolidated using same batches of carbide powders.

Barantseva and Paderno [6] suggested that the CTE of the solid solutions are lower as compared to the single carbides (both TaC and HfC). They argued that maximum in CTE observed for TaC–HfC and NbC–ZrC system was comparable with data for electrical resistivity in these specimens. Thus it was assumed that behavior of CTE of the solid-solutions (**Figs. S8, S9**) is due to local electron distribution in the solid-solution. The reduction in number of electrons must be accompanied by the an increase in the number of electrons localized in the atom nuclei and participating in the covalent. The bond energy of Hf to C (in HfC) (16.45 eV) compared to Tato C (in TaC) (16.92 eV) [7].

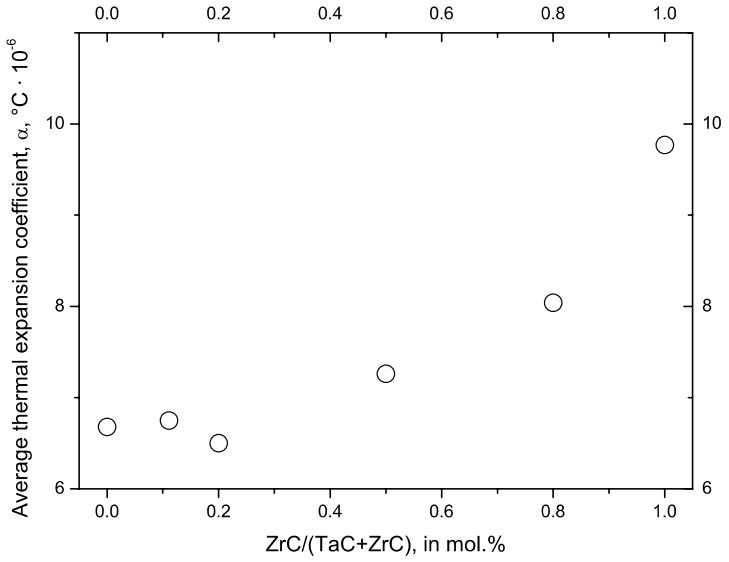

Fig. S6. Concentration dependence of the coefficient of thermal expansion of solid-solutions and monolithic carbides in the ZrC – TaC system (1500–2000°C). [4].

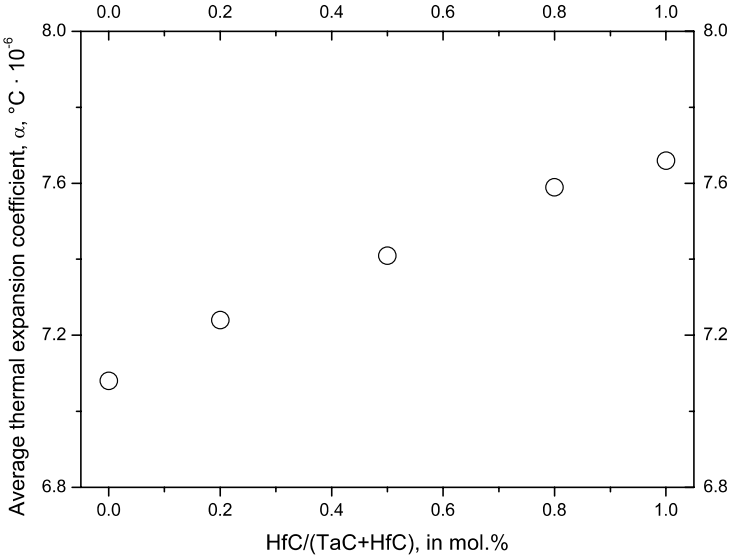

Fig. S7. Concentration dependence of the coefficient of thermal expansion of solid-solutions and monolithic carbides in the HfC–TaC system (RT–2000°C). [5].

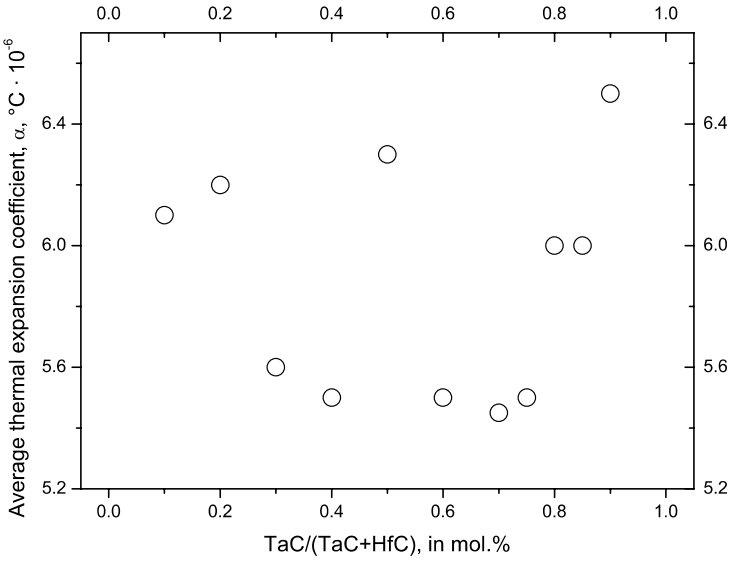

Fig. S8. Concentration dependence of the coefficient of thermal expansion of solid-solutions and monolithic carbides in the HfC–TaC system (accuracy 1.5%). [6].

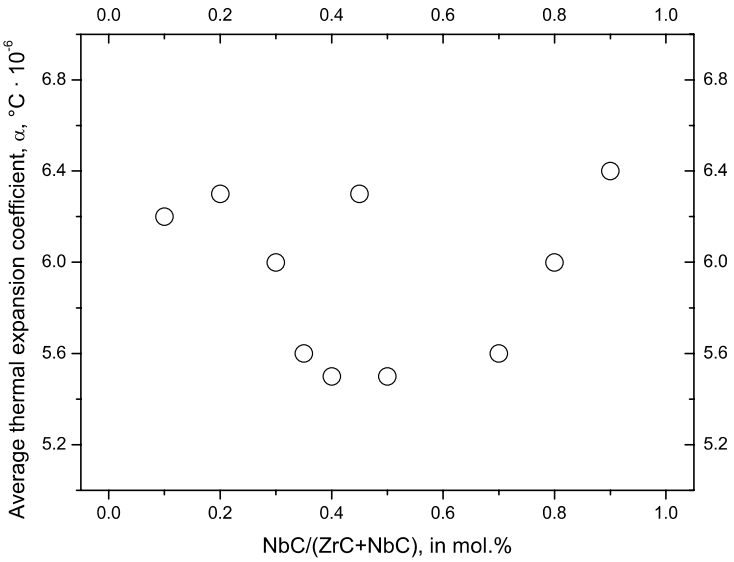

Fig. S9. Concentration dependence of the coefficient of thermal expansion of solid-solutions and monolithic carbides in the NbC–ZrC system (accuracy 1.5%). [6].

References

[1] Andrievski RA, Spivak II. Strength of Refractory Compounds. Chelyabinsk(USSR): Metallurgiya; 1989 [in Russian].

[2] Döbelin N, Kleeberg R. Profex: a graphical user interface for the Rietveld refinement program BGMN. *J Appl Crystallogr*. 2015;**48**:1573–1580.

[3] Toby BH, Von Dreele, RB. GSAS-II: the genesis of a modern open-source all purpose crystallography software package. 2013);**46**(2):544–549.

[4] Miccioli BR, Shaffer PTB. High- Temperature Thermal Expansion Behavior of Refractory Materials- I, Selected Monocarbides and Binary Carbides. *J Am Ceram Soc.* 1964;**47**[7]:351–356.

[5] Cedillos-Barraza O, Grasso S, Al Nasiri N, et al. Sintering behaviour, solid solution formation and characterisation of TaC, HfC and TaC–HfC fabricated by spark plasma sintering. *J Eur Ceram Soc.* 2016;**36**:1539–1548.

[6] Barantseva IG, Paderno VN. Thermal expansion of solid solutions in thesystems ZrC–NbC and HfC–TaC. in: Samsonov GV editor. Refractory Carbides. London (UK): Consultants Bureau; 1974, pp. 283–285.

[7] Pierson HO. Handbook of Refractory Carbides and Nitrides: Properties, Characteristics, Processing, and Applications. Westwood (NJ): Noyes Publications; 1996, p. 340.